An algebraic restoration method for estimating fixed-pattern noise in infrared imagery from a video sequence

Ünal Sakoğlu[a]*, Russell C. Hardie[b], Majeed M. Hayat[a], Bradley M. Ratliff[a] and J. Scott Tyo[a]

[a]Department of Electrical and Computer Engineering, University of New Mexico, Albuquerque, NM, USA 87131-0001

[b]Department of Electrical and Computer Engineering, University of Dayton, Dayton, OH, USA 45469-0226

ABSTRACT

The inherent nonuniformity in the photoresponse and readout-circuitry of the individual detectors in infrared focal-plane-array imagers result in the notorious fixed-pattern noise (FPN). FPN generally degrades the performance of infrared imagers and it is particularly problematic in the midwavelength and longwavelength infrared regimes. In many applications, employing signal-processing techniques to combat FPN may be preferred over hard calibration (e.g., two-point calibration), as they are less expensive and, more importantly, do not require halting the operation of the camera. In this paper, a new technique that uses knowledge of global motion in a video sequence to restore the true scene in the presence of FPN is introduced. In the proposed setting, the entire video sequence is regarded as an output of a motion-dependent linear transformation, which acts collectively on the true scene and the unknown bias elements (which represent the FPN) in each detector. The true scene is then estimated from the video sequence according to a minimum mean-square-error criterion. Two modes of operation are considered. First, we consider non-radiometric restoration, in which case the true scene is estimated by performing a regularized minimization, since the problem is ill-posed. The other mode of operation is radiometric, in which case we assume that only the perimeter detectors have been calibrated. This latter mode does not require regularization and therefore avoids compromising the radiometric accuracy of the restored scene. The algorithm is demonstrated through preliminary results from simulated and real infrared imagery.

Keywords: focal plane arrays, infrared photodetectors, nonuniformity correction, fixed-pattern noise

1. INTRODUCTION

Focal-plane-array (FPA) sensors typically exhibit spatial nonuniformity among the array elements. This nonuniformity results in the so-called fixed-pattern noise (FPN), which is superimposed on the on the true image degrading the quality and radiometric accuracy of the image.[1] This is particularly a serious problem for the FPAs that work in the mid-wave and long-wave infrared (IR), and hence, for thermal imagers. In the past two decades, various techniques have been proposed and used to remedy this nonuniformity problem. The most basic and effective solution for correcting nonuniformity is the radiometric calibration of the camera, where the camera is exposed to one or more spatially-constant and known irradiation sources. The most common examples are the one-point calibration and the two-point calibration.[1–3] The calibration process can be as simple as dropping a constant-temperature shutter in front of the camera's field-of-view (FOV), or it could involve the use of a black-body source, operated at multiple temperatures. Although calibration is generally a good solution to the nonuniformity problem, it is undesirable for several reasons. First, one needs to perform the calibration as frequently as needed, which is dictated by the speed at which the nonuniformity drifts over time. Thus, to do the calibration, one needs to sacrifice the use of camera at calibration times. Second, good calibration often requires the use of one or more black-body sources, which are expensive and require their own electrical and mechanical hardware for their control and interface with the camera. As a result of the often complex and always disruptive nature of calibration, techniques that achieve nonuniformity correction by means of post-processing are highly motivating and attractive in many applications. These techniques are often referred to as "scene-based"

*E-mail: sakoglu@ece.unm.edu, Telephone: 1 505 277-1259

nonuniformity correction (NUC) techniques, since they do not require imaging special scenes obtained from the calibration source for the purpose of calibration.

To date, two main categories of post-processing NUC techniques have been developed: (1) statistical techniques and (2) algebraic techniques. The statistical techniques model the FPN as a random spatial noise and estimate the statistics of the noise to remove it.[4–9] The algebraic techniques, on the other hand, make use of global motion between the frames in the video sequence and attempt to compensate for the nonuniformity by means of algebraic methods without making statistical assumptions about the FPN.[10–20] The approach proposed in this paper belongs to the second category. In particular, the rationale of the proposed approach is based on the approach proposed earlier by Ratliff *et al.*,[17,18] which exploits global motion in a video sequence in conjunction with a bilinear-interpolation model for motion to unify all the biases of the array (or convert the biases to zero when the algorithm is operated in a radiometric mode in which case the perimeter detectors are first calibrated). However, the current work puts the aforementioned technique in a general matrix-algebra framework that allows the utilization of minimum-mean-square-error principles as well as the employment of versatile regularization techniques. This generalization may prove to be better suited to handle scenarios for which gain nonuniformity noise or bilinear-interpolation-approximation errors for motion are severe.

2. FIXED-PATTERN NOISE MODEL

Each photo-detector element of the FPA converts the photonic energy into electrical energy by converting the irradiance information into voltage or current information, which can be modeled as a function of the input irradiance. Knowing the detectors' precise characteristics would solve the spatial nonuniformity problem since it enables us to extract the real irradiance, viz., the real image, from the measured FPA readout. Unfortunately, such input-output characteristics of detectors vary from detector to detector, even though they are fabricated under identical conditions. Although extreme care is taken to manufacture detectors that have similar properties (such as response transfer function, spectral response characteristics, etc.) each detector has different characteristics. Even the characteristics of the same detector might drift over time because of changes in external conditions and it generally cannot be modeled accurately in a deterministic fashion.

As commonly practiced, the simplest way to characterize the input-output relation is the use of a linear-response model, which includes the gain and bias of the photodetector. For any detector, we can write

$$y = az + b,$$

where z is the true irradiance, a is the gain, b is the bias, and y is the observed quantity (usually, current or voltage). Assume that an FPA has MxN detectors, where M is the number of rows and N is the number of columns. For nth frame in the video sequence Φ and for the i,jth pixel, we can write

$$y_n(i,j) = a(i,j)z_n(i,j) + b(i,j)$$

Note that in the above model we have not included the temporal noise. Also note that the gain and biases in each pixel, $a(i,j)$ and $b(i,j)$, do not change within the sequence Φ. Finally, we will assume that the gain a is constant among all detectors (and hence we can set it to unity without loss of generality). This latter assumption is commonly practiced and it is due to the observation that in many operational conditions, the bias nonuniformity typically dominates gain nonuniformity. With these simplifying assumptions, our model reduces to

$$y_n(i,j) = z_n(i,j) + b(i,j), \quad i = 1,...,M,\ j = 1,...,N. \tag{1}$$

Observe that in the above equation, there are MN equations and the only known quantity are the measurements $y_n(i,j)$. Thus, there are a total of $2MN$ unknowns.

In one-point calibration, we first apply a known constant illumination z on all pixels and calculate the bias response $b(i,j) = z_n(i,j) - y_n(i,j)$. To do this, the camera's operation is halted, a black-body source is inserted in front of the camera's FOV, and the $b(i,j)$ are calculated for all (i,j). These calculated biases are subtracted from the imagery in the sequence Φ accordingly yielding bias correction. However, if calibration is to be avoided, the general question is how can Eqn.1 be solved to get $z_n(i,j)$s without having any a-priori information about

$b(i,j)$s. Realizing that we have $2MN$ unknowns and only MN equations, to solve for the $z_n(i,j)$'s, we need another set of equations. Such new set can be $y_m(i,j) = L(z_n + b)$, where L is some new linear transformation of $z_n(i,j)$ and $b(i,j)$, $i = 1, ..., M, j = 1, ..., N$. The transformation (or operator) L is assumed to represent a physical process, and $y_m(i,j)$ are the corresponding results that we can physically observe. An example of such physical process is translational movement of the camera, which yields global translational motion of the scene. In the next section, we will exploit this representation to yield estimates of the unknown biases.

2.1. Modeling the 2-dimensional global shift

We will assume that the motion between the frames n and m, where $m > n$, is a simple translational shift. Usually IR-cameras are operated at rates of 30 or 60 frames/sec. Assuming a realistic motion of the user, which is human or a mechanical rotating device, the shifts between frames are usually sub-pixel shifts. We will discuss this case in the next sub-section and the super-pixel case is discussed in 2.1.2. In our paper, we assume that the algorithm is provided with frames that exhibit global rigid shift motion and that we know the amount of vertical and horizontal shift. This knowledge of motion is obtained through the use of standard motion estimation algorithms. In this paper we use the gradient-based shift estimation algorithm reported in.[21, 22]

2.1.1. Sub-pixel shift model

Following Ratliff *et al.*,[18] we begin with the frame n and assume (without loss of generality) downward-right motion of the camera. Denoting the vertical shift between two frames with α, and horizontal shift with β, we can express the shifted frame m as

$$\begin{aligned} y_m(i,j) &= (1-\alpha)(1-\beta)z_n(i,j) + \alpha(1-\beta)z_n(i+1,j) \\ &+ \beta(1-\alpha)z_n(i,j+1) + \alpha\beta z_n(i+1,j+1) + b(i,j), \end{aligned} \tag{2}$$

for $i = 1, ..., M-1$ and $j = 1, ..., N-1$. Therefore we obtain $(M-1)(N-1)$ additional equations in addition to the MN equations in Eqn.1, which yields a total of $2MN - (M+N-1)$ equations. Recall that we had $2MN$ known quantities, namely, the $y_n(i,j)$'s and the $y_m(i,j)$'s. Also, when we reach the boundaries, where $i = M, \text{or} j = N$, we cannot use Eqn.2, and we are therefore in need of $M+N-1$ additional equations. We can overcome this situation in two ways. (1) The non-radiometric way and (2) the radiometric way. In the former, we impose a constraint on the bias values. For example, by relying on the physical fact that the average bias over all detector elements is approximately is zero, we may introduce the constraint that the bias at the end of each row is the sum of the negative of all the remaining biases in the row. A similar constraint can be applied to biases at the bottom of each column. This constraint is non-radiometric since we do not utilize any radiometric calibration, but make a physical, statistical assumption for the biases of the perimeter pixels. Accordingly, we introduce the following constraints:

$$\begin{aligned} b(M,j) &= -\sum_{i=1}^{M-1} b(i,j), j = 1, ..., N-1, \\ b(i,N) &= -\sum_{j=1}^{N-1} b(i,j), i = 1, ..., M-1, \text{ and} \\ b(M,N) &= \sum_{i=1}^{M-1}\sum_{j=1}^{N-1} b(i,j). \end{aligned} \tag{3}$$

These equations provide us extra $M+N-1$ equations we need. Thus, by means of the above constraints we reduce the number of unknown biases by $M+N-1$, which results in the same number of equations and unknowns in the system described by Eqns.1 through 3. We can therefore solve for the perimeter irradiance, that is $z_n(i,j)$, for $i = M$ and $j = N$, by means of Eqn.1.

For the radiometric way, we may use the fact that biases on the perimeter of the array have already been calibrated a priori (see Ratliff *et al.*[18] for details of the notion of partial perimeter calibration) from radiometric-calibration so that $b(M,j) = b(i,N) = b(M,N) = 0$ for $i = 1, \ldots, M-1$ and $j = 1, \ldots, N-1$.

We next discuss the case for which the shifts are general (i.e., not only subpixel).

2.1.2. The general case: super-pixel shift model

If the camera motion is sufficiently fast, there can be global super-pixel shift between the frames for which $\alpha > 1$ or $\beta > 1$. In this case Eqn. 3 must be modified. For example, if the horizontal shift is $\alpha = 1.55$, and the vertical shift is $\beta = 2.70$, then the last 3 rows and last 2 rows are the perimeter pixels. This means, for the non-radiometric case, the constraint must be applied to the biases $b(i, j)$ for $i = M-2, M-1, M$ and $j = N-1, N$. For the radiometric case, on the other hand, the radiometrically estimated bias values for these perimeter pixels are needed. We define $\lfloor\alpha\rfloor$ and $\lfloor\beta\rfloor$ to be the nearest integers, towards zero, to α and β, respectively. With this notation, we can write the modified version of Eqn.3 as:

$$\begin{aligned}
b(M-\lfloor\alpha\rfloor, j) = ... = b(M, j) &= -\sum_{i=1}^{M-\lfloor\alpha\rfloor-1} b(i, j), \quad j = 1, ..., N-\lfloor\beta\rfloor-1, \\
b(i, N-\lfloor\beta\rfloor) = ... = b(i, N) &= -\sum_{j=1}^{N-\lfloor\beta\rfloor-1} b(i, j), \quad i = 1, ..., M-\lfloor\alpha\rfloor-1, \text{ and} \\
b(M-\lfloor\alpha\rfloor : M\,,\, N-\lfloor\beta\rfloor : N) &= \sum_{i=1}^{M-\lfloor\alpha\rfloor-1} \sum_{j=1}^{N-\lfloor\beta\rfloor-1} b(i, j),
\end{aligned} \tag{4}$$

where $(M-\lfloor\alpha\rfloor : M\,,\, N-\lfloor\beta\rfloor : N)$ denotes all pairs (i, j) for $i = M-\lfloor\alpha\rfloor, ..., M$ and $j = N-\lfloor\beta\rfloor, ..., N$.

2.1.3. Matrix equation model for the non-radiometric case

The system of equations 2-4 can be written in matrix form as:

$$\mathbf{Y} = \mathbf{AD}, \tag{5}$$

where

$$\mathbf{Y} = \begin{bmatrix} Y_n \\ Y_m \end{bmatrix}, \ \mathbf{D} = \begin{bmatrix} Z \\ B \end{bmatrix}, \ \mathbf{A} = \begin{bmatrix} I_{MN\mathbf{x}MN} & R_{MN\mathbf{x}(M-\lfloor\alpha\rfloor-1)(N-\lfloor\beta\rfloor-1)} \\ A_{(M-\lfloor\alpha\rfloor-1)(N-\lfloor\beta\rfloor-1)\mathbf{x}MN} & I_{(M-\lfloor\alpha\rfloor-1)(N-\lfloor\beta\rfloor-1)\mathbf{x}(M-\lfloor\alpha\rfloor-1)(N-\lfloor\beta\rfloor-1)} \end{bmatrix},$$

$$Y_n = \begin{bmatrix} y_n(1,1) \\ \vdots \\ y_n(M,1) \\ y_n(1,2) \\ \vdots \\ y_n(M,2) \\ \\ \vdots \\ \\ y_n(1,N) \\ \vdots \\ y_n(M,N) \end{bmatrix}_{MN\mathbf{x}1} \quad Y_m = \begin{bmatrix} y_m(1,1) \\ \vdots \\ y_m(M-\lfloor\alpha\rfloor-1,1) \\ y_m(1,2) \\ \vdots \\ y_m(M-\lfloor\alpha\rfloor-1,2) \\ \\ \vdots \\ \\ y_m(1,N-\lfloor\beta\rfloor-1) \\ \vdots \\ y_m(M-\lfloor\alpha\rfloor-1,N-\lfloor\beta\rfloor-1) \end{bmatrix}_{(M-\lfloor\alpha\rfloor-1)(N-\lfloor\beta\rfloor-1)\mathbf{x}1}$$

$$Z = \begin{bmatrix} z(1,1) \\ \vdots \\ z(M,1) \\ z(1,2) \\ \vdots \\ z(M,2) \\ \\ \vdots \\ \\ z(1,N) \\ \vdots \\ z(M,N) \end{bmatrix}_{MN\mathbf{x}1} \quad B = \begin{bmatrix} b(1,1) \\ \vdots \\ b(M-\lfloor\alpha\rfloor-1,1) \\ b(1,2) \\ \vdots \\ b(M-\lfloor\alpha\rfloor-1,2) \\ \\ \vdots \\ \\ b(1,N-\lfloor\beta\rfloor-1) \\ \vdots \\ b(M-\lfloor\alpha\rfloor-1,N-\lfloor\beta\rfloor-1) \end{bmatrix}_{(M-\lfloor\alpha\rfloor-1)(N-\lfloor\beta\rfloor-1)\mathbf{x}1}$$

In the above equations, R is the appropriate matrix that governs the zero-mean constraint and A is the weight matrix that governs the shift estimation. Defining $\alpha' = 1-\alpha$ and $\beta' = 1-\beta$, these matrices can be recast as

$$A = \begin{bmatrix}
\alpha'\beta' & \alpha\beta' & 0 & \dots & 0 & 0 & \alpha'\beta & \alpha\beta & 0 & \dots & 0 & 0 & & & \cdots & & & 0 & 0 & 0 & 0 & 0 & 0 \\
0 & \alpha'\beta' & \alpha\beta' & 0 & \dots & 0 & 0 & \alpha'\beta & \alpha\beta & 0 & \dots & 0 & & & \cdots & & & 0 & 0 & 0 & 0 & 0 & 0 \\
\vdots & & \ddots & & & \vdots & \vdots & & & \ddots & & \vdots & & & & & & & & \vdots & & & \\
0 & 0 & \dots & 0 & \alpha'\beta' & \alpha\beta' & 0 & \dots & 0 & 0 & \alpha'\beta & \alpha\beta & & & \cdots & & & 0 & 0 & 0 & 0 & 0 & 0 \\
 & & & & & \ddots & & & & & & \ddots & & & & & & & & \vdots & & & \\
0 & 0 & 0 & 0 & 0 & 0 & & & \cdots & & & & \alpha'\beta' & \alpha\beta' & 0 \dots 0 & 0 & \alpha'\beta & \alpha\beta & 0 & \dots & 0 & 0 \\
0 & 0 & 0 & 0 & 0 & 0 & & & \cdots & & & & 0 & \alpha'\beta' & \alpha\beta' & 0 \dots 0 & 0 & \alpha'\beta & \alpha\beta & 0 & \dots & 0 \\
 & & & \vdots & & & & & & & & & \vdots & & \ddots & & \vdots & \vdots & & \ddots & & \vdots \\
0 & 0 & 0 & 0 & 0 & 0 & & & \cdots & & & & 0 & 0 & \dots 0 & \alpha'\beta' & \alpha\beta' & 0 & \dots & 0 & 0 & \alpha'\beta & \alpha\beta
\end{bmatrix}$$

$\leftarrow N - \lfloor\beta\rfloor - 1$ row blocks of width $M - \lfloor\alpha\rfloor - 1$

$\uparrow N$ column blocks of width M

$$R = \begin{bmatrix}
1 & \dots & 0 & 0 & \dots & 0 & \cdots & 0 & \dots & 0 \\
\vdots & \ddots & \vdots & \vdots & \ddots & \vdots & \ddots & \vdots & \ddots & \vdots \\
0 & \dots & 1 & 0 & \dots & 0 & \cdots & 0 & \dots & 0 \\
-1 & \dots & -1 & 0 & \dots & 0 & \cdots & 0 & \dots & 0 \\
\vdots & \ddots & \vdots & \vdots & \ddots & \vdots & \ddots & \vdots & \ddots & \vdots \\
-1 & \dots & -1 & 0 & \dots & 0 & \cdots & 0 & \dots & 0 \\
 & & & & & & & & & \\
0 & \dots & 0 & 1 & \dots & 0 & \cdots & 0 & \dots & 0 \\
\vdots & \ddots & \vdots & \vdots & \ddots & 0 & \ddots & 0 & \dots & 0 \\
0 & \dots & 0 & 0 & \dots & 1 & \cdots & 0 & \dots & 0 \\
0 & \dots & 0 & -1 & \dots & -1 & \cdots & 0 & \dots & 0 \\
\vdots & \ddots & \vdots & \vdots & \ddots & \vdots & \ddots & \vdots & \ddots & \vdots \\
0 & \dots & 0 & -1 & \dots & -1 & \cdots & 0 & \dots & 0 \\
 & & & & & & & & & \\
 & \vdots & & & \vdots & & \ddots & & \vdots & \\
 & & & & & & & & & \\
0 & \dots & 0 & 0 & \dots & 0 & \cdots & 1 & \dots & 0 \\
\vdots & \ddots & \vdots & \vdots & \ddots & \vdots & \ddots & \vdots & \ddots & \vdots \\
0 & \dots & 0 & 0 & \dots & 0 & \cdots & 0 & \dots & 1 \\
0 & \dots & 0 & 0 & \dots & 0 & \cdots & -1 & \dots & -1 \\
\vdots & \ddots & \vdots & \vdots & \ddots & \vdots & \ddots & \vdots & \ddots & \vdots \\
0 & \dots & 0 & 0 & \dots & 0 & \cdots & -1 & \dots & -1 \\
 & & & & & & & & & \\
-1 & \dots & 0 & -1 & \dots & 0 & \cdots & -1 & \dots & 0 \\
\vdots & \ddots & \vdots & \vdots & \ddots & \vdots & \ddots & \vdots & \ddots & \vdots \\
0 & \dots & -1 & 0 & \dots & -1 & \cdots & 0 & \dots & -1 \\
1 & \dots & 1 & 1 & \dots & 1 & \cdots & 1 & \dots & 1 \\
\vdots & \ddots & \vdots & \vdots & \ddots & \vdots & \ddots & \vdots & \ddots & \vdots \\
1 & \dots & 1 & 1 & \dots & 1 & \cdots & 1 & \dots & 1 \\
 & & & & & & & & & \\
 & \vdots & & & \vdots & & \ddots & & \vdots & \\
 & & & & & & & & & \\
-1 & \dots & 0 & -1 & \dots & 0 & \cdots & -1 & \dots & 0 \\
\vdots & \ddots & \vdots & \vdots & \ddots & \vdots & \ddots & \vdots & \ddots & \vdots \\
0 & \dots & -1 & 0 & \dots & -1 & \cdots & 0 & \dots & -1 \\
1 & \dots & 1 & 1 & \dots & 1 & \cdots & 1 & \dots & 1 \\
\vdots & \ddots & \vdots & \vdots & \ddots & \vdots & \ddots & \vdots & \ddots & \vdots \\
1 & \dots & 1 & 1 & \dots & 1 & \cdots & 1 & \dots & 1
\end{bmatrix}.$$

$M - \lfloor\alpha\rfloor - 1$ rows of $1's$

$\lfloor\alpha\rfloor + 1$ rows of $-1's$

this block repeats $\lfloor\beta\rfloor + 1$ times

$\uparrow N - \lfloor\beta\rfloor - 1$ column blocks of width $M - \lfloor\alpha\rfloor - 1$

2.1.4. Matrix equation model for the radiometric case

In the radiometric mode of the algorithm, the bias values in the perimeter pixels are assumed to be known through radiometric calibration and there is no need for constraint as in the non-radiometric case discussed earlier. The algorithm corrects the perimeter pixels using the precise values of the biases. Therefore, the entries that are -1 in the first $(N - \lfloor\beta\rfloor - 1)M$ rows and all the non-zero entries in the last $(\lfloor\beta\rfloor + 1)M$ rows become 0. Aside from this, the matrix equation model is same as in Eqn. 5.

Direction	Pre-operation	Post-operation
$(\alpha > 0, \beta > 0)$	none	none
$(\alpha > 0, \beta < 0)$	rotate frames counterclockwise 90°, swap(α, β)	rotate frames clockwise 90°
$(\alpha < 0, \beta > 0)$	rotate frames clockwise 90°, swap(α, β)	rotate frames counterclockwise 90°
$(\alpha < 0, \beta < 0)$	rotate frames 180°	rotate frames 180°

Table 1. List of pre- and post-operations for different directions of shift.

2.2. Solution to the matrix equation

Clearly, the solution to Eqn.5 is $\hat{\mathbf{D}} = \mathbf{A}^{-1}\mathbf{Y}$, which also trivially minimizes the error represented by the cost function $\|\mathbf{Y}-\mathbf{AD}\|$ (which is zero in this case). However, for the non-radiometric case, we introduce an additional penalization term on the error in the estimation of the bias values. We define regularized least-squares cost function as

$$C(\mathbf{D}) = \|Y - \mathbf{AD}\|^2 + \|\mathbf{FD}\|^2, \tag{6}$$

where

$$\mathbf{F} = \begin{bmatrix} \epsilon\mathbf{F}_Z & \mathbf{0} \\ \mathbf{0} & \lambda\mathbf{F}_B \end{bmatrix}, \tag{7}$$

$\mathbf{F}_Z$ is a high-pass (Laplacian) operator matrix that operates on Z, ϵ is the corresponding weight, $\mathbf{F}_B$ is a low-pass (smoothing) operator matrix that operates on B, and λ is the corresponding weight. Note that by adding the term $\|\mathbf{FD}\|^2$ to the cost function, the following types of solutions are penalized: (1) The fluctuation in the estimated irradiance, since we expect irradiance to have low spatial variance, (2) smoothness in the estimated bias, since we expect bias to have high spatial variance. The solution that minimizes Eqn. 6 is

$$\hat{\mathbf{D}} = (\mathbf{A}^T\mathbf{A} + \mathbf{F}^T\mathbf{F})^{-1}\mathbf{A}^T\mathbf{Y}. \tag{8}$$

Thus, by utilizing Eqn. 3, one can solve for the bias values at the perimeters and can correct for the future frames (whose indices are in Φ) by using

$$z_k(i,j) = y_k(i,j) - b(i,j), \;\; i = 1, ..., M, \;\; j = 1, ..., N, \;\; k \in \Phi.$$

The algorithm can be repeated for each set of frames.

To improve the estimation within a frames set, one can repeat the estimation for many pairs of frames and average the resulting estimated bias. A multi-frame approach can also be used in which more than two frames are used for estimation. In the latter case, using all of the possible frame combinations would give the optimal result; however, it would require extensive computation as the matrices become prohibitively large .

Finally, note that the matrix equations that are written so far are for the right-downward camera motion. However, the estimation for the motions in the other three directions can be solved using the same set of equations after rotating the frames in an appropriate manner, swapping the vertical and horizontal shift parameters if necessary, applying the algorithm, and rotating back the frames. In Table 1, the pre- and post-operations to be done prior to and after the application of the algorithm are listed.

3. APPLICATIONS AND RESULTS

3.1. Application to simulated data

The algorithm was first applied to a simulated frame pair. A 32-by-32 gray level image, shown in Fig. 1(a), was considered. The image pixels have values between 0 and 255. The gray level of the background is 192, and the gray level just around the letters "NUC" has value 225. The darkest level of the letters is 76. In Fig. 1(b), a frame simulated with bilinear interpolation model for down-rightward shift with parameters $\alpha = 0.70$ and $\beta = 1.55$ is shown. We picked these shift parameters to simulate both sub-pixel and super-pixel shift in the same example. We then added bias non-uniformity as shown in Fig. 1(c), utilizing zero-mean Gaussian-distributed

random variables with each with a standard deviation of 4. We used the true shift values in the algorithm, and the results are discussed below.

For the radiometric case, we obtained perfect results as expected without the need for any regularization, as shown in Fig. 1(d). For the non-radiometric case, our algorithm estimated the biases very well too, as presented in Fig. 2, which should be compared to Fig. 1(c). Estimation results with different values of the regularization parameter λ, for $\lambda = 10, 2, 0.5$ and 0, are shown in Fig. 2. We see from Fig. 2(d) that the regularization is necessary for the estimation with non-radiometric perimeter calibration. As a measure of error, we calculated the standard deviation of the error in estimating the true irradiance (hence the bias values) as 2.67, 2.63, 5.40 and 124.12 for $\lambda = 10, 2, 0.5$ and 0, respectively. In general, the estimation results for $\lambda \simeq 2$ were the best visually and had the least error standard deviation, as we see in Fig. 2(b). For the case $\lambda = 0.5$, as shown in Fig. 2(c), we can see a pattern in the direction of the camera motion. This is characteristic of error in predicting the perimeter bias values through the constraint equations.

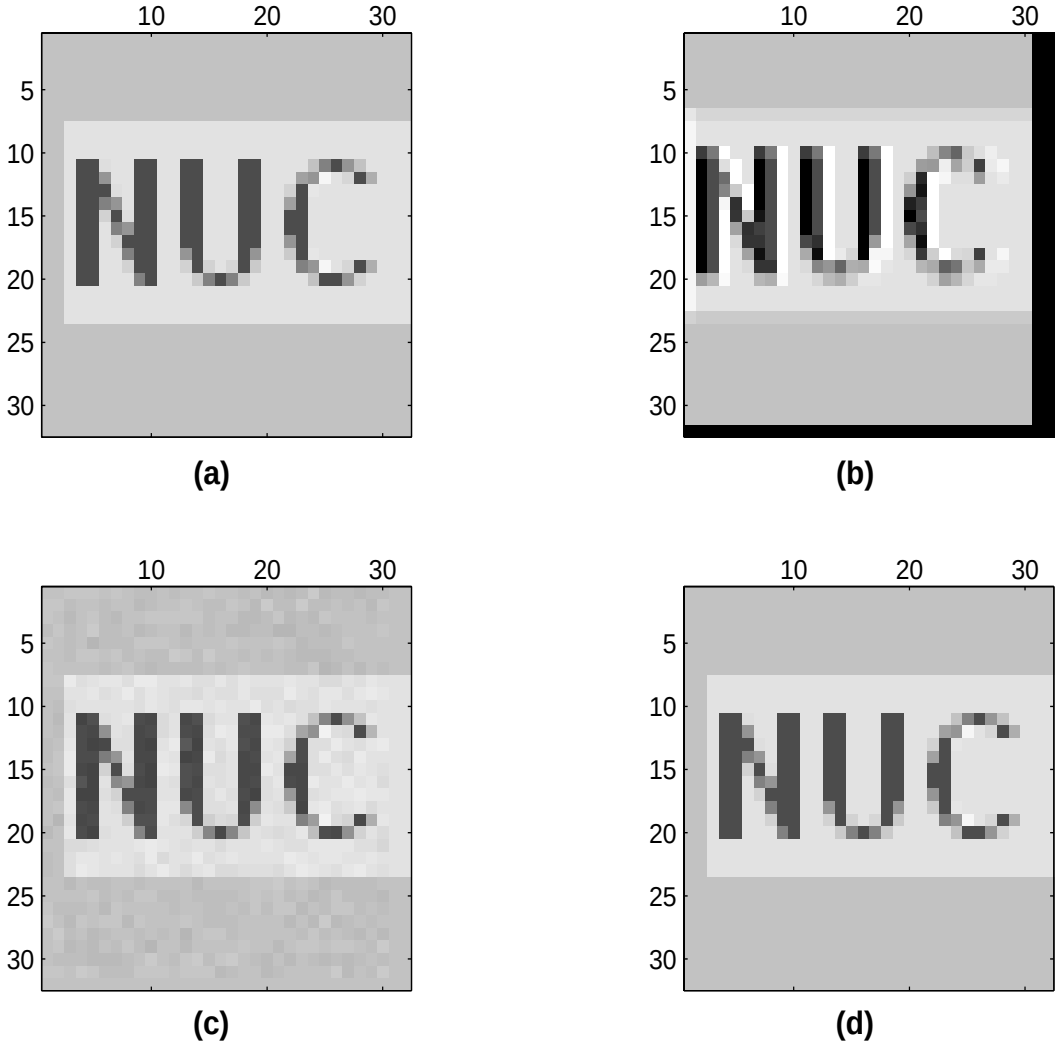

Figure 1. (a) First frame. (b) Second frame, which is a shifted version of the first frame resulting from 1.55-right, 0.70-downward camera motion. (c) First frame with bias non-uniformity added. The standard deviation of the bias nonuniformity is 4. (d) Estimation of the first frame with radiometric calibration applied to the perimeter pixels.

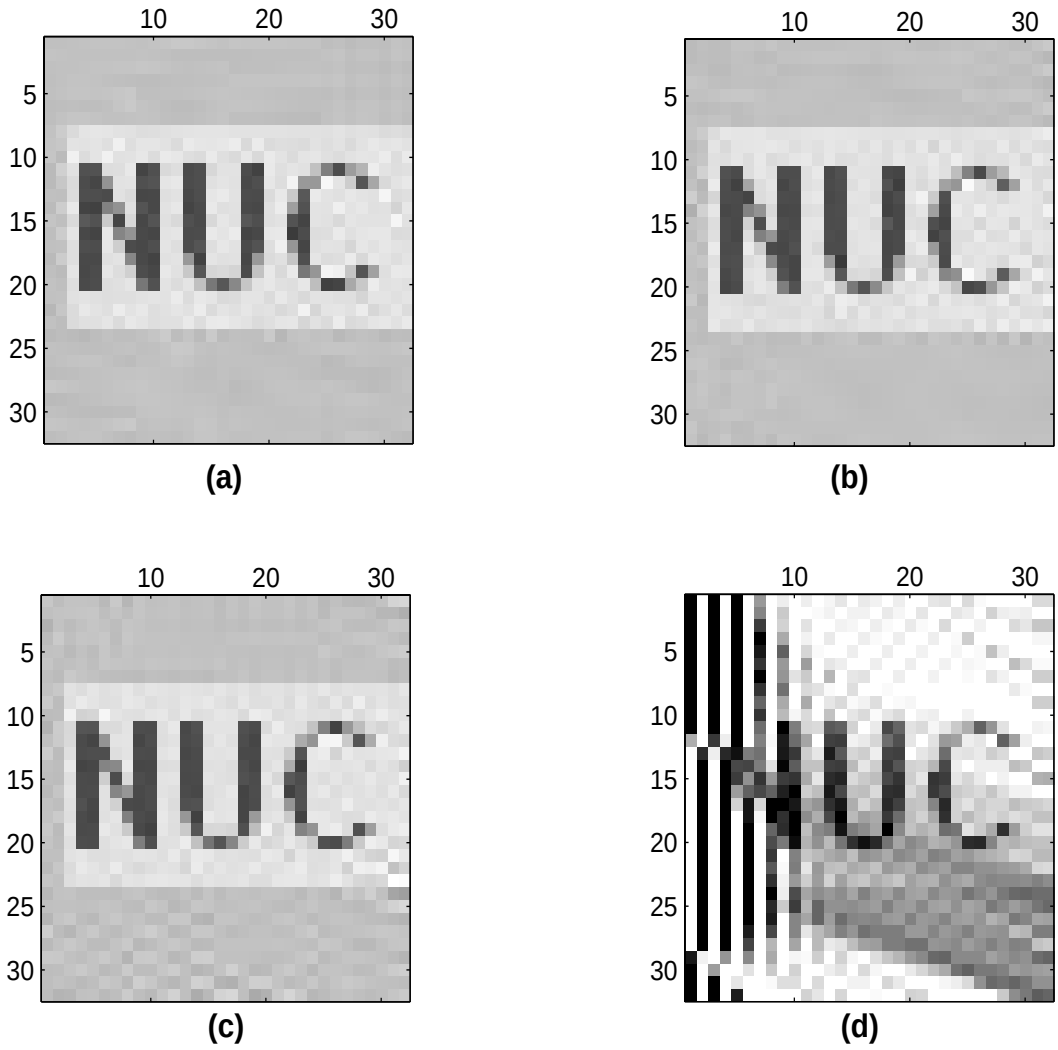

Figure 2. Non-radiometric estimation for the same shift values and same level of bias nonuniformity as in Fig. 1 for: (a) $\lambda = 10$ (b) $\lambda = 2$ (c) $\lambda = 0.5$ (d) $\lambda = 0$

3.2. Application to real data

We applied the algorithm on a 48-by-48 pixel subimage of video sequence taken with an IR-camera (InSb FPA). The video sequence had 512 frames, and we picked frames 487s and 488, as shown in Figs. 3(a) and (b), respectively. The estimated shifts between the frames were 0.276-downward and 0.365-rightward. We applied our algorithm in both the radiometric and non-radiometric modes. From our experience on simulated data, we picked $\lambda = 2$ for the non-radiometric version. In Figs. 3(a) and (b) we see the observed frames, corrupted with the bias nonuniformity. The one-pixel-thick perimeter of frame 1 is calibrated. As a bench mark, we show in Fig. 3(c) the estimate of the true scene obtained through radiometric-calibration (namely, a 2-point calibration). In Fig. 3(d), we show result of our radiometric mode of algorithm. In contrast, in Fig. 3(e) we show the results of the non-radiometric mode of the algorithm. In both corrected images shown in Fig. 3(d) and (e), the non-uniformity has almost disappeared. However, in Fig. 3(d) we see a pattern in the direction of the motion, which stems from the fact that the error in the perimeter biases propagate in the error of the inner bias values along the direction of the motion. The main reason is that the bilinear-interpolation model for shift does not model real shifts exactly, therefore it leads to errors that further propagate along the direction of the motion. This effect also appears in other registration-based NUC algorithms[17,18] and can be reduced through diversity in the

motion direction by averaging the corrections from multiple frames. Note that this is an extreme test for the algorithm since we only utilize one pair of frames. The performance is expected to improve as corrections from different pairs of frames are obtained and averaged.

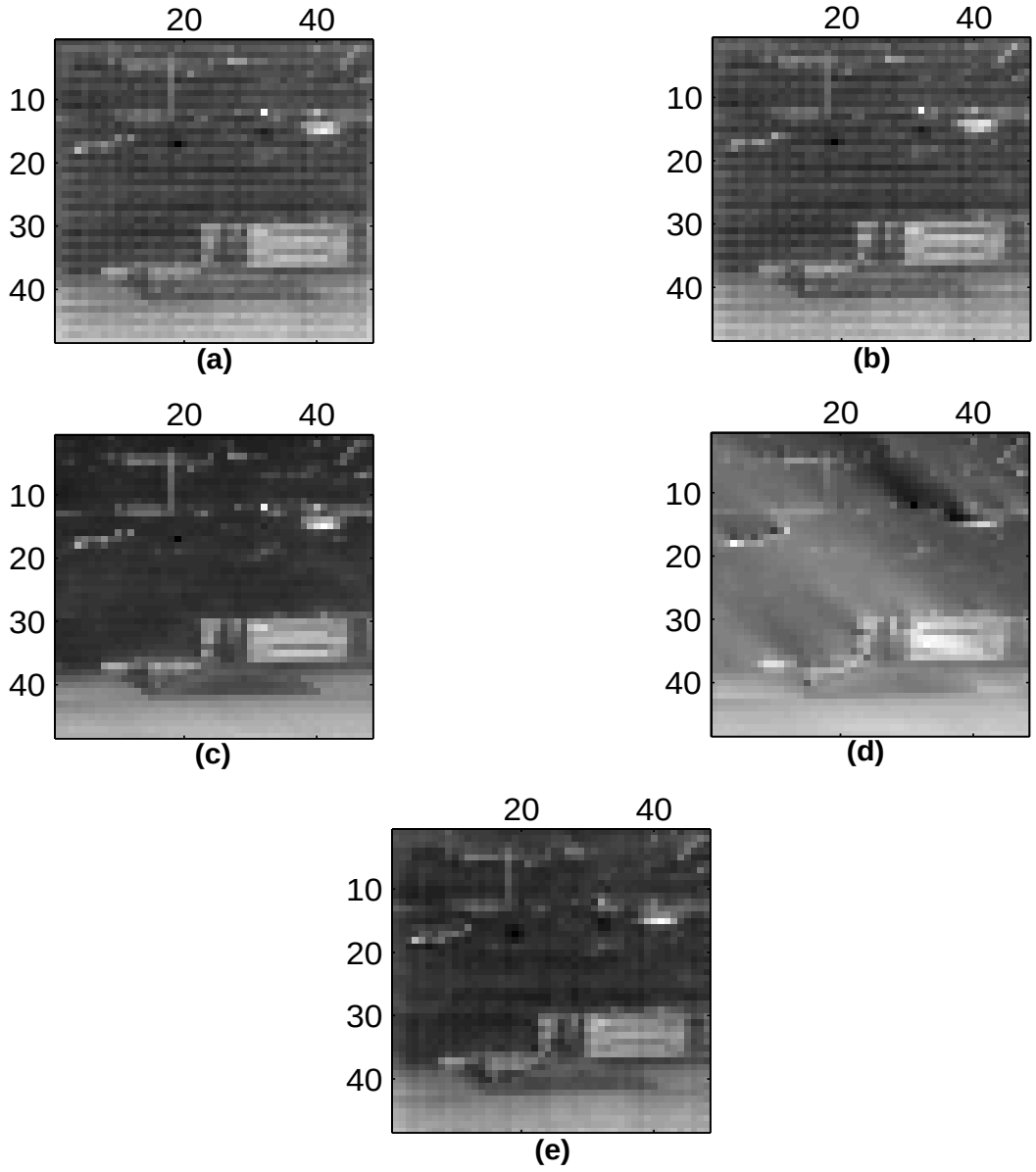

Figure 3. (a) First frame. (b) Second frame, shifted as a result of 0.365-right, 0.276-downward camera motion. (c) correction of the first frame using a 2-point calibration. (d) Correction using the algorithm in the radiometric mode. (e) Correction using the algorithm in the non-radiometric mode.

3.3. Computational issues: sparse matrices

The computational complexity of the algorithm is considerably high due to the large sizes of the system matrices and the inversions involved. For an image of size M-by-N, the matrix to be inverted in Eqn. 8 is on the order of 2MN-by-2MN. For an image of size 128-by-128, the dimension of $\mathbf{A}$ is approximately 2^{15}-by-2^{15}. The remedy to the computational complexity is exploiting the sparsity of the matrix $\mathbf{A}$. Normally, with double precision, the

storage of **A** for 128-by-128 image would require about $2^{33} \approx 8$ GB of memory. However, **A** is not only sparse, but also many of its entries are 1s. The number of nonzero elements is MN+6(M-1)(N-1) and MN+2(M-1)(N-1) of them are 1s. For instance, in the sub-pixel-shift case, examples of the fraction r(M,N) of the number of nonzero elements to all elements are: r(32,32)≃0.00172, r(48,48)≃0.000764, r(64,64)≃0.000429, r(128,128)≃0.000107, and r(256,256)≃0.0000267. Another remedy to the computational complexity problem is the structure of the system matrix. The matrix R has a multiple-bordered block-diagonal form[23] and it can be represented as a Kronecker product of two simple multiple-bordered diagonal-form matrices. The matrix A is a bi-diagonal block Toeplitz matrix,[24] which is obtained via addition of two Kronecker products of smaller bi-diagonal Toeplitz matrices. The aforementioned structural and sparseness properties of the system matrix motivate us to exploit sparse-matrix techniques to remedy the computational burden.[25] We anticipate reduction factor in the matrix inversion time in the range of 10–100 if a direct-inversion technique is used. Additionally, we would also obtain a reduction in the memory requirements if an iterative inversion method is used.[26]

4. CONCLUSIONS

In this paper, we reported a new technique for bias nonuniformity correction that uses knowledge of global motion in a video sequence. In the proposed setting, the entire video sequence is regarded as an output of a motion-dependent linear transformation, which acts collectively on the true scene and the unknown bias elements in each detector. The proposed approach exploits the rationale proposed earlier by Ratliff *et al.*[17,18] and puts it in a general matrix-algebra framework that allows the utilization of minimum-mean-square-error principles as well as the employment of versatile regularization techniques. The true scene is then estimated from the video sequence according to a minimum mean-square-error criterion. Two modes of operation are considered: a radiometric and non-radiometric modes. The algorithms performs perfectly on simulated data for which the global motion is induced according to a bilinear-interpolation model. Although the algorithm was successful in removing the bulk of the fixed-pattern noise in real data, it exhibited certain striping artifacts along the direction of motion. This effect is attributed to errors in the inaccuracy of the bilinear-interpolation model for motion. We emphasize that this is an extreme test for the algorithm since only one pair of frames was employed in extracting the bias correction matrix. The algorithm can easily be extended so that it uses additional frame pairs from the video sequence in order to diversify the direction of global shifts. For example, the correction matrix resulting from individual pairs of frames can be averaged yielding an overall bias-correction matrix that exhibits reduced striping artifacts. Due to the need for inverting a large matrix, the algorithm is computationally intensive. However, by exploiting the sparsity of the matrix (which is on the order of 10^{-4}) it may be possible to reduce the computation time by factor of 10 to 100.

REFERENCES

1. A. F. Milton, F. R. Barone, and M. R. Kruer, "Influence of nonuniformity on infrared focal plane array performance," *Optical Engineering* **24**(5), pp. 855–862, 1985.
2. J. M. Mooney, F. D. Shepherd, W. S. Ewing, J. E. Murguia, and J. Silverman, "Responsivity nonuniformity limited performance of infrared staring cameras," *Optical Engineering* **28**, pp. 1151–1161, 1989.
3. D. L. Perry and E. L. Dereniak, "Linear theory of nonuniformity correction in infrared staring sensors," *Optical Engineering* **32**(8), pp. 1853–1859, 1993.
4. P. M. Narendra, "Reference-free nonuniformity compensation for IR imaging arrays," in *Proceedings of the SPIE: Smart Sensors II*, **252**, pp. 10–17, The International Society for Optical Engineering, 1980.
5. P. M. Narendra and N. A. Foss, "Shutterless fixed pattern noise correction for infrared imaging arrays," in *Proceedings of the SPIE: Technical Issues in Focal Plane Development*, **282**, pp. 44–51, The International Society for Optical Engineering, 1981.
6. J. G. Harris, "Continuous-time calibration of VLSI sensors for gain and offset variations," in *Proceedings of the SPIE: Smart Focal Plane Arrays and Focal Plane Array Testing*, M. Wigdor and M. A. Massie, eds., **2474**, pp. 23–33, The International Society for Optical Engineering, May 1995.
7. J. G. Harris and Y.-M. Chiang, "Minimizing the ghosting artifact in scene-based nonuniformity correction," in *Proceedings of the SPIE: Infrared Imaging Systems: Design, Analysis, Modeling, and Testing IX*, G. C. Holst, ed., **3377**, pp. 106–113, The International Society for Optical Engineering, Aug. 1998.

8. M. M. Hayat, S. N. Torres, S. C. Cain, and E. Armstrong, "Model-based real-time nonuniformity correction in focal plane array detectors," in *Proceedings of the SPIE: Infrared Imaging Systems: Design, Analysis, Modeling, and Testing IX*, G. C. Holst, ed., **3377**, pp. 122–132, The International Society for Optical Engineering, Aug. 1998.
9. M. M. Hayat, S. N. Torres, E. E. Armstrong, S. C. Cain, and B. J. Yasuda, "Statistical algorithm for nonuniformity correction in focal-plane arrays," *Applied Optics* **38**, pp. 772–780, Feb. 1999.
10. W. F. O'Neil, "Dithered scan detector compensation," in *Proceedings of the Infrared Information Symposium (IRIS) Specialty Group on Passive Sensors*, 1993.
11. W. F. O'Neil, "Experimental verification of dithered scan nonuniformity correction," in *Proceedings of the Infrared Information Symposium (IRIS) Specialty Group on Passive Sensors*, **1**, pp. 329–339, 1997.
12. R. C. Hardie, M. M. Hayat, E. E. Armstrong, and B. J. Yasuda, "Scene-based nonuniformity correction with video sequences and registration," *Applied Optics* **39**, pp. 1241–1250, Mar. 2000.
13. B. M. Ratliff, "An algebraic scene-based algorithm for nonuniformity correction in focal plane arrays," master's thesis, University of Dayton, Dayton, OH, Dec. 2001.
14. B. M. Ratliff, M. M. Hayat, and R. C. Hardie, "Algebraic scene-based nonuniformity correction in focal plane arrays," in *Proceedings of the SPIE: Infrared Imaging Systems: Design, Analysis, Modeling, and Testing XII*, G. C. Holst, ed., **4372**, pp. 114–124, The International Society for Optical Engineering, (Orlando, FL), Sept. 2001.
15. B. M. Ratliff, M. M. Hayat, and J. S. Tyo, "On the performance of a radiometrically-calibrated nonuniformity correction algorithm," **IX**, pp. 14–18, Proceedings of the 6th World Multiconference on Systemics, Cybernetics and Informatics, (Orlando, FL), July 2002. Invited.
16. B. M. Ratliff, M. M. Hayat, and J. S. Tyo, "Radiometrically calibrated scene-based nonuniformity correction for infrared array sensors," in *Proceedings of the SPIE: Infrared Technology and Applications XXVIII*, B. F. Andresen, G. F. Fulop, and M. Strojnik, eds., **4820**, pp. 359–367, The International Society for Optical Engineering, (Seattle, WA), Jan. 2003.
17. B. M. Ratliff, M. M. Hayat, and R. C. Hardie, "An algebraic algorithm for nonuniformity correction in focal plane arrays," *Journal of the Optical Society of America A* **19**, pp. 1737–1747, Sept. 2002.
18. B. M. Ratliff, M. M. Hayat, and J. S. Tyo, "Radiometrically accurate scene-based nonuniformity correction for array sensors," *Journal of the Optical Society of America A* **20**, pp. 1890–1899, Oct. 2003.
19. B. M. Ratliff, M. M. Hayat, and J. S. Tyo, "Algorithm for radiometrically accurate nonuniformity correction with arbitrary scene motion," in *Proceedings of the SPIE: Infrared Imaging Systems: Design, Analysis, Modeling, and Testing XIV*, G. C. Holst, ed., **5076**, pp. 82–91, The International Society for Optical Engineering, (Orlando, FL), Aug. 2003.
20. B. M. Ratliff, M. M. Hayat, and J. S. Tyo, "Generalized algebraic nonuniformity correction algorithm," *JOSA A, submitted April 2004* .
21. M. Irani and S. Peleg, "Improving resolution by image registration," *CVGIP - Graphical Models and Image Processing* **53**(3), pp. 231–239, 1991.
22. R. C. Hardie, K. J. Barnard, J. G. Bognar, E. E. Armstrong, and E. A. Watson, "High-resolution image reconstruction from a sequence of rotated and translated frames and its application to an infrared imaging system," *Optical Engineering* **37**(1), pp. 247–260, 1998.
23. J. K. Reid, ed., *Large Sparse Sets of Linear Equations*, Academic Press, London, UK, 1971.
24. G. H. Golub and C. F. V. Loan, *Matrix Computations*, The Johns Hopkins University Press, Baltimore, Maryland, 3rd ed., 1996.
25. D. S. Watkins, *Fundamentals of Matrix Computations*, John Wiley and Sons, Inc., New York, 2nd ed., 2002.
26. I. S. Duff, ed., *Sparse Matrices and their Uses*, Academic Press, London, UK, 1981.